An anisotropic equation of state for solid solutions, with application to plagioclase

R. Myhill[1]*

[1]School of Earth Sciences, University of Bristol. Wills Memorial Building, Queen's Road, Bristol BS8 1RJ

SUMMARY

This paper presents a framework for building anisotropic equations of state for solid solutions. The framework satisfies the connections between elastic and thermodynamic properties required by Maxwell's reciprocal relations. It builds on a recent anisotropic equation of state for pure phases under small deviatoric stresses, adding a dependence on a vector $\boldsymbol{n}$, whose components n_i contain the molar amounts of independent endmembers in a solid solution. These endmembers may have distinct chemical compositions, site species occupancies or electronic spin states. The high albite-anorthite (C$\bar{1}$) plagioclase solid solution is used to illustrate the formulation.

Key words: Equations of state – Elasticity and anelasticity – Seismic anisotropy

1 INTRODUCTION

Solid solutions can be thought of as mixtures of different endmembers, each of which have fixed structure, composition and distribution of species on sites. In traditional hydrostatic thermodynamic models, the Gibbs/Helmholtz energy is expressed as a function of pressure/volume, temperature and endmember proportions (e.g. Helffrich & Wood, 1989; Holland & Powell, 2003; Stixrude & Lithgow-Bertelloni, 2005; Myhill & Connolly, 2021). Derivatives of the Gibbs energy with respect to these

* bob.myhill@bristol.ac.uk

Table 1. Symbols used in this paper.

Symbol	Units	Description
$\mathcal{E}, \mathcal{F}, \mathcal{G}, \mathcal{H}$	J	Internal energy, Helmholtz energy, Gibbs energy, Enthalpy
$\boldsymbol{M}, M_{ij}$	m	Extensive cell tensor
$\ln_{\mathrm{M}} \boldsymbol{M}, (\ln_{\mathrm{M}} \boldsymbol{M})_{ij}$	[unitless]	Matrix logarithm of extensive cell tensor relative to a 1 m^3 cube ($\boldsymbol{M}/\boldsymbol{I}$)
$\boldsymbol{F}, F_{ij}$	[unitless]	Deformation gradient tensor
$\boldsymbol{\varepsilon}, \varepsilon_{ij}$	[unitless]	Small strain tensor
V	m^3	Volume
T, T_{ref}	K	Temperature, Reference temperature
$\boldsymbol{n}, n_i$	mol	Molar amounts of compositional/structural endmembers
$\boldsymbol{p}, p_i$	[unitless]	Molar proportions of endmembers ($\boldsymbol{n}/\boldsymbol{1n}$)
$\boldsymbol{\sigma}, \sigma_{ij}$	Pa	Cauchy ("true") stress
P	Pa	Pressure ($-\delta_{ij}\sigma_{ij}/3$)
P_{th}	Pa	Thermal pressure
$\mathbb{S}_{\mathrm{T}}, S_{\mathrm{T}ijkl}, S_{\mathrm{T}pq}$	Pa^{-1}	Isothermal compliance tensor (standard and Voigt form)
$\mathbb{C}_{\mathrm{T}}, C_{\mathrm{T}ijkl}, C_{\mathrm{T}pq}$	Pa	Isothermal stiffness tensor (standard and Voigt form)
$\boldsymbol{\alpha}, \alpha_{ij}; \alpha_V$	K^{-1}	Thermal expansivity tensor; Volumetric thermal expansivity
$\beta_{\mathrm{TR}}, \beta_{\mathrm{NR}}$	Pa^{-1}	Isothermal and isentropic Reuss compressibilities
$K_{\mathrm{TR}}, K_{\mathrm{NR}}$	Pa	Isothermal and isentropic Reuss bulk moduli
Ψ, Ψ_{ijkl}	[unitless]	Anisotropic state tensor
$\boldsymbol{1}, 1_i$		Vector of ones (used for summation)
$\boldsymbol{I}, \delta_{ij}$		Identity matrix / Kronecker delta
$\ln_{\mathbf{M}}()$		Matrix logarithm function
$\exp_{\mathbf{M}}()$		Matrix exponential function

variables yield physical properties including the volume/pressure, entropy, thermal expansivity, Reuss bulk modulus and isobaric and hydrostatic-isochoric heat capacities.

Partial derivatives of the Gibbs/Helmholtz energies with respect to pressure/volume cannot provide anisotropic physical properties such as thermal expansivities and elastic moduli. For this, partial derivatives must instead be taken as a function of stress or strain. In Myhill (2022), I presented an anisotropic equation of state for pure, isochemical substances. The equation of state was designed so that it could be used in conjunction with any traditional hydrostatic equation of state, with the new parameters defining only the anisotropic properties. In this paper, I extend that equation of state to solid solutions. Symbols used in this paper are given in Table 1.

2 CELL TENSORS, DEFORMATION AND REFERENCE FRAMES

2.1 The standard state cell tensor

At a given reference state (usually 1 bar, 298.15 K), the unit cell of each endmember in a solid solution can be defined using vector lengths and angles (a, b, c, α, β and γ). These are reference frame-invariant - that is, none of the values depend on the orientation of the crystal relative to the frame of reference. However, a frame of reference must be defined when considering deformation of the unit cell in an equation of state, so it is convenient to also define the unit cell in that frame of reference. In the feldspar example used in this study, we adopt the convention of Brown et al. (2016), where the y axis of the Cartesian reference frame is aligned parallel to the crystallographic b axis in the standard state, the x axis is perpendicular to the b and c axes, and the z axis is chosen to satisfy a right-handed coordinate system. Using this convention, we can define a reference state molar "cell tensor" $\boldsymbol{M}_0$ [m/mol]:

$$\boldsymbol{M}_0 = \left(\frac{N_A}{Z}\right)^{\frac{1}{3}} \begin{bmatrix} a\sqrt{\sin^2(\gamma) - n_2^2} & 0 & 0 \\ a\cos(\gamma) & b & c\cos(\alpha) \\ an_2 & 0 & c\sin(\alpha) \end{bmatrix} \tag{1}$$

$$n_2 = \frac{\cos(\beta) - \cos(\alpha)\cos(\gamma)}{\sin(\alpha)} \tag{2}$$

where Z is the number of unit cells per formula unit. Each column of this tensor represents a vector from the origin to an adjacent vertex of a parallelepiped. This parallelepiped has the shape of the unit cell and a volume equal to the molar volume of the material V_0.

At standard temperature and pressure, triclinic albite (NaAlSi$_3$O$_8$, C$\bar{1}$) has unit cell parameters $a = 8.1366(2) \cdot 10^{-10}$ m, $b = 12.7857(2) \cdot 10^{-10}$ m, $c = 7.1582(3) \cdot 10^{-10}$ m, $\alpha = 94.253(2)°$, $\beta = 116.605(2)°$, $\gamma = 87.756(2)°$ and $Z = 4$ (Brown et al., 2016). These values lead to the following reference state cell tensor:

$$\boldsymbol{M}_0 = \begin{pmatrix} 0.038701 & 0 & 0 \\ 0.001695 & 0.068018 & -0.002824 \\ -0.019312 & 0 & 0.037975 \end{pmatrix} \tag{3}$$

yielding a molar volume $V_0 = \det(\boldsymbol{M}_0) = 99.965$ cm^3/mol.

2.2 The deformation gradient tensor and its derivatives

Deformation of a cell tensor from $\boldsymbol{M}_0$ to a state $\boldsymbol{M}$ is achieved by applying a deformation gradient tensor $\boldsymbol{F}$ to the reference state cell tensor $\boldsymbol{M_0}$

$$M_{ik} = F_{ij}M_{0jk} \tag{4}$$

The deformation gradient tensor $\boldsymbol{F}$ and its time derivative $\dot{\boldsymbol{F}}$ describe the transformation of local particle positions from their initial state $\boldsymbol{x}_0$ to a final state $\boldsymbol{x}$:

$$F_{ij} = \frac{\partial x_i}{\partial x_{0j}}, \; \dot{F}_{ij} = \frac{\partial \dot{x}_i}{\partial x_{0j}} \tag{5}$$

The velocity gradient tensor $\dot{\boldsymbol{L}}$ represents the change in velocity of particles relative to their current positions:

$$\dot{L}_{ij} = \frac{\partial \dot{x}_i}{\partial x_j} = \dot{F}_{ik} F_{kj}^{-1} \tag{6}$$

The velocity gradient tensor can be asymmetric even if the deformation gradient tensor is always symmetric (Section 2.3). Infinitesimal strain rate $\dot{\boldsymbol{\varepsilon}}$ and spin $\dot{\boldsymbol{\omega}}$ tensors can be defined as the symmetric and antisymmetric parts of $\dot{\boldsymbol{L}}$:

$$\dot{\varepsilon}_{ij} = \frac{1}{2} \left(\dot{L}_{ij} + \dot{L}_{ji} \right) \tag{7}$$

$$\dot{\omega}_{ij} = \frac{1}{2} \left(\dot{L}_{ij} - \dot{L}_{ji} \right) \tag{8}$$

The infinitesimal strain rate can be decomposed into temperature and stress-related terms:

$$\dot{\varepsilon}_{ij} = \alpha_{ij} \dot{T} + S_{\mathrm{T}ijlm} \dot{\sigma}_{lm} \tag{9}$$

$$= \alpha_{ij} \dot{T} - \beta_{\mathrm{T}ij} \dot{P} + S_{\mathrm{T}ijlm} \dot{\tau}_{lm} \tag{10}$$

where $\boldsymbol{\alpha}$, $\boldsymbol{\beta}_T$ and $\mathbb{S}_T$ are the thermal expansivity, isothermal compressibility and elastic compliance tensors. Stress $\boldsymbol{\sigma}$ is positive under tension, pressure P is positive under compression and $\boldsymbol{\tau}$ is the deviatoric stress:

$$\sigma_{ij} = -P \delta_{ij} + \tau_{ij} \tag{11}$$

Using Equations 6, 7 and 9, the thermal expansivity and isothermal compressibility can be written as

$$\alpha_{ij} = \frac{1}{2} \left(\left(\frac{\partial F_{ik}}{\partial T} \right)_P F_{kj}^{-1} + \left(\frac{\partial F_{jk}}{\partial T} \right)_P F_{ki}^{-1} \right) \tag{12}$$

$$\beta_{\mathrm{T}ij} = -\frac{1}{2} \left(\left(\frac{\partial F_{ik}}{\partial P} \right)_T F_{kj}^{-1} + \left(\frac{\partial F_{jk}}{\partial P} \right)_T F_{ki}^{-1} \right) \tag{13}$$

$$= \frac{\beta_{\mathrm{RT}}}{2} \left(\left(\frac{\partial F_{ik}}{\partial \ln V} \right)_T F_{kj}^{-1} + \left(\frac{\partial F_{jk}}{\partial \ln V} \right)_T F_{ki}^{-1} \right) \tag{14}$$

$$\beta_{\mathrm{RT}} = \beta_{\mathrm{T}ij} \delta_{ij} = -\left(\frac{\partial \ln V}{\partial P} \right)_{\mathrm{T}} \tag{15}$$

where β_{RT} is the isothermal Reuss compressibility. Hydrostatically deformed orthotropic materials in a rotation-free coordinate frame will have eigenvectors of $\boldsymbol{F}$ which are constant with respect to pressure and temperature. In such cases $\dot{\boldsymbol{F}}$ and $\boldsymbol{F}^{-1}$ are commutative, and the velocity gradient tensor can be written (Haber, 2018) $\dot{L}_{ij} = (\ln_{\mathrm{M}} \dot{\boldsymbol{F}})_{ik}$ and the expressions for $\boldsymbol{\alpha}$ and $\boldsymbol{\beta}_T$ simplify considerably

(Myhill, 2022):

$$\alpha_{ij} = \left(\frac{\partial (\ln_{\mathrm{M}} \boldsymbol{F})_{ik}}{\partial T} \right)_P \tag{16}$$

$$\beta_{\mathrm{T}ij} = -\left(\frac{\partial (\ln_{\mathrm{M}} \boldsymbol{F})_{ik}}{\partial P} \right)_T = \beta_{\mathrm{RT}} \left(\frac{\partial (\ln_{\mathrm{M}} \boldsymbol{F})_{ik}}{\partial \ln V} \right)_T \tag{17}$$

2.3 Rotation in non-orthotropic systems

Under hydrostatic conditions, conservation of angular momentum implies that any infinitesimal deformation will be rotation-free, and therefore that $\dot{\boldsymbol{L}}$ will always be symmetric. Unfortunately, in non-orthotropic systems (monoclinic and triclinic), a symmetric $\dot{\boldsymbol{L}}$ does not guarantee a symmetric deformation gradient tensor in $\boldsymbol{F}$. Asymmetry, and the finite rotation implied by that asymmetry, arises when the eigenvectors of strain change during deformation. Figure 1 illustrates this by means of a two-step pure-shear deformation of an initially square object. The incremental strain at each step is shown between the objects, and the finite deformation gradients after each step are shown inside the objects. In Figure 1a, the box is first shortened along the y-axis, and then shortened along an axis inclined from the vertical. Note that even though every transitional strain is rotation-free (i.e., symmetric), the second phase of deformation produces an asymmetric deformation gradient tensor.

In the anisotropic equation of state presented by Myhill (2022), $\boldsymbol{F}$ is calculated as a function of volume and temperature, and is always symmetric. This means that increments in strain ($\dot{\boldsymbol{L}}$) will be asymmetric, as shown in Figure 1b, which illustrates the same deformation as in Figure 1a. Thermal expansivity, isothermal compressibility and isothermal compliance tensors must be calculated taking this into account (Equations 12 and 14 and Section 3.2.1).

3 FORMULATION

3.1 Volumetric equations of state

The anisotropic equation of state presented in this paper can be built on top of any equation of state for which molar volume can be found as a function of pressure P, temperature T and independent endmember proportions $\boldsymbol{p}$:

$$V = V(P, T, \boldsymbol{p}) \tag{18}$$

This includes models such as those in (Stixrude & Lithgow-Bertelloni, 2011), where the endmember equation of state is actually formulated as $P(V, T)$, or the Helmholtz (elastic) solution models advocated by Myhill (2018). In most solution models in the geological literature, the calculation of the

(a) Zero angular velocity ($\dot{\boldsymbol{L}}$ always symmetric)

$$\begin{bmatrix} 1.00 & 0.00 \\ 0.00 & 1.00 \end{bmatrix} \qquad \xrightarrow{} \qquad \begin{bmatrix} 1.00 & 0.00 \\ 0.00 & 0.75 \end{bmatrix} \qquad \xrightarrow{} \qquad \begin{bmatrix} 1.00 & 0.22 \\ 0.30 & 0.56 \end{bmatrix}$$

$$\begin{bmatrix} 1.00 & 0.00 \\ 0.00 & 0.75 \end{bmatrix} \qquad\qquad\qquad \begin{bmatrix} 1.00 & 0.30 \\ 0.30 & 0.75 \end{bmatrix}$$

(b) Zero net rotation ($\boldsymbol{F}$ always symmetric)

$$\begin{bmatrix} 1.00 & 0.00 \\ 0.00 & 1.00 \end{bmatrix} \qquad \xrightarrow{} \qquad \begin{bmatrix} 1.00 & 0.00 \\ 0.00 & 0.75 \end{bmatrix} \qquad \xrightarrow{} \qquad \begin{bmatrix} 1.01 & 0.25 \\ 0.25 & 0.55 \end{bmatrix}$$

$$\begin{bmatrix} 1.00 & 0.00 \\ 0.00 & 0.75 \end{bmatrix} \qquad\qquad \begin{bmatrix} 1.01 & 0.34 \\ 0.25 & 0.73 \end{bmatrix}$$

Figure 1. Rotations arising from rotation-free strain in non-orthotropic materials. (a) Two phases of pure shear deformation are imposed on a square of material. The eigenvectors of deformation are different for each step. A rotation emerges. (b) The same deformation as in (a), but the second phase of deformation involves a component of simple shear (pure shear and a rotation), such that the deformation gradient tensor remains rotation free. Dotted outline shows the result from (a).

volume is split into endmember and excess contributions:

$$V(P, T, \boldsymbol{p}) = p_i V_i(P, T) + p_i p_j W_{ij}^V(P, T) + \dots \tag{19}$$

where p_i is the proportion of independent endmember i in the solution, V_i is the volume of that endmember and W_{ij}^V are volumetric interaction terms between endmembers. Endmember volumes may be determined directly from P and T, or the endmember equations of state may be formulated as a function of volume, in which case the correct volume at any given pressure may be found by iteration.

3.2 The anisotropic equation of state

3.2.1 Endmembers

In Myhill (2022), I showed that self-consistent anisotropic properties for pure phases could be modelled by using a fourth order symmetric anisotropic tensor $\Psi(V, P_{\text{th}}(V, T))$, with parameters that sat-

isfied the condition:

$$\ln\left(\frac{V}{V_0}\right) = \Psi_{ijkl}\delta_{ij}\delta_{kl} \tag{20}$$

In that paper, the anisotropic tensor was used to define the deformation gradient tensor and the isothermal compliance tensor:

$$F_{ij} = (\exp_{\mathbf{M}} \Psi \boldsymbol{I})_{ij} \tag{21}$$

$$\frac{S_{\mathrm{T}ijkl}}{\beta_{\mathrm{RT}}} = \left(\frac{\partial\psi_{ijkl}}{\partial\ln V}\right)_T \tag{22}$$

The constraint given by Equation (20) ensures that the anisotropic equation of state remains consistent with the volumetric equation of state (Section 3.1), as a result of the mathematical identity (Petersen & Pedersen, 2012):

$$\det\boldsymbol{F} = \exp(\mathrm{Tr}(\ln_{\mathbf{M}}\boldsymbol{F})) \tag{23}$$

and physical identities:

$$\det\boldsymbol{F} = \frac{V}{V_0} \tag{24}$$

In Myhill (2022), I focused mainly on orthotropic materials (the equation of state was demonstrated by orthorhombic forsterite). For these materials, Equations 21 and 22 are consistent with each other because:

$$\frac{\beta_{\mathrm{T}ij}}{\beta_{\mathrm{RT}}} = \frac{\partial(\ln_{\mathbf{M}}\boldsymbol{F})_{ij}}{\partial\ln V} = \Psi_{ijkl}\delta_{kl} = \frac{S_{\mathrm{T}ijkl}}{\beta_{\mathrm{RT}}}\delta_{ij} \tag{25}$$

For non-orthotropic materials, this is no longer the case; because of rotation (Equation 13 and Section 2.3):

$$\frac{\beta_{\mathrm{T}ij}}{\beta_{\mathrm{RT}}} = \frac{1}{2}\left(\left(\frac{\partial F_{ik}}{\partial\ln V}\right)_T F_{kj}^{-1} + \left(\frac{\partial F_{jk}}{\partial\ln V}\right)_T F_{ki}^{-1}\right) \tag{26}$$

For monoclinic and triclinic systems, Equation 22 can be replaced with Equation 26 and the following equations:

$$\frac{S_{\mathrm{T}ijkl}}{\beta_{\mathrm{RT}}} = \left(\frac{\partial\psi_{ijkl}}{\partial\ln V}\right)_T \quad \text{when three or four indices } (i, j, k, l) \text{ are the same} \tag{27}$$

$$= \left(\frac{\partial\psi_{ijkl}}{\partial\ln V}\right)_T \quad \text{when } i \neq j \text{ and } k \neq l \tag{28}$$

$$S_{\mathrm{T}iijj} = \frac{1}{2}(-S_{\mathrm{T}iiii} - S_{\mathrm{T}jjjj} + S_{\mathrm{T}kkkk} + \beta_{\mathrm{T}ii} + \beta_{\mathrm{T}jj} - \beta_{\mathrm{T}kk}) \tag{29}$$

$$S_{\mathrm{T}iijk} = 2\beta_{\mathrm{T}jk} - S_{\mathrm{T}jjjk} - S_{\mathrm{T}kkjk} \tag{30}$$

The indices in the last two equations signify different index values (e.g. $i = 1$, $j = 3$, $k = 2$); no summation is implied. The factor 2 in Equation 30 arises from the multiplication of individual

compliances required in the conversion to the Voigt form of the compliance tensor. The modified terms occupy the positions coloured blue (Equation 29) and red (Equation 30) in the following matrix:

$$
\begin{pmatrix}
S_{\mathrm{T}1111} & \textcolor{blue}{S_{\mathrm{T}1122}} & \textcolor{blue}{S_{\mathrm{T}1133}} & \textcolor{red}{S_{\mathrm{T}1123}} & S_{\mathrm{T}1113} & S_{\mathrm{T}1112} \\
\textcolor{blue}{S_{\mathrm{T}2211}} & S_{\mathrm{T}2222} & \textcolor{blue}{S_{\mathrm{T}2233}} & S_{\mathrm{T}2223} & \textcolor{red}{S_{\mathrm{T}2213}} & S_{\mathrm{T}2212} \\
\textcolor{blue}{S_{\mathrm{T}3311}} & \textcolor{blue}{S_{\mathrm{T}3322}} & S_{\mathrm{T}3333} & S_{\mathrm{T}3323} & S_{\mathrm{T}3313} & \textcolor{red}{S_{\mathrm{T}3312}} \\
\textcolor{red}{S_{\mathrm{T}2311}} & S_{\mathrm{T}2322} & S_{\mathrm{T}2333} & S_{\mathrm{T}2323} & S_{\mathrm{T}2313} & S_{\mathrm{T}2312} \\
S_{\mathrm{T}1311} & \textcolor{red}{S_{\mathrm{T}1322}} & S_{\mathrm{T}1333} & S_{\mathrm{T}1323} & S_{\mathrm{T}1313} & S_{\mathrm{T}1312} \\
S_{\mathrm{T}1211} & S_{\mathrm{T}1222} & \textcolor{red}{S_{\mathrm{T}1233}} & S_{\mathrm{T}1223} & S_{\mathrm{T}1213} & S_{\mathrm{T}1212}
\end{pmatrix}
\tag{31}
$$

3.2.2 Solid solutions

At any given composition, solid solutions must obey the same self-consistency rules as the endmembers. One way to ensure this is to define the standard state molar cell tensor $\boldsymbol{M}_0$ and deformation gradient tensor $\boldsymbol{F}$ as follows:

$$
\boldsymbol{M} = \boldsymbol{F}\boldsymbol{M}_0
\tag{32}
$$

$$
\ln_{\mathrm{M}} \boldsymbol{M}_0(\boldsymbol{p}, n) = p_m(\ln_{\mathrm{M}}(\boldsymbol{M}_{0m})) + \frac{\ln(n)}{3}\boldsymbol{I}
\tag{33}
$$

$$
\ln_{\mathrm{M}} \boldsymbol{F}(V_{\mathrm{mol}}, T, \boldsymbol{p}) = p_m(\ln_{\mathrm{M}} \boldsymbol{F}_m(V_{\mathrm{mol}}, T)) + (\ln_{\mathrm{M}} \boldsymbol{F})_{\mathrm{xs}}(V_{\mathrm{mol}}, T, \boldsymbol{p})
\tag{34}
$$

where V_{mol} is the molar volume, n is the total number of moles of substance and $\boldsymbol{p}$ is the vector of molar fractions of the independent species. The $_m$ subscript refers to the mth endmember in the solution. The following equality must be satisfied:

$$
(\ln_{\mathrm{M}} \boldsymbol{F})_{\mathrm{xs}ij}\delta_{ij} = 0
\tag{35}
$$

The reference molar volume and relative volume change at any composition can then be found from $\boldsymbol{M}_0$ using the identities given by Equations 23 and 24:

$$
V_0(\boldsymbol{p}) = \exp(p_m \operatorname{Tr}(\ln_{\mathrm{M}}(\boldsymbol{M}_{0m}))) = \prod_m V_{0m}^{p_m}
\tag{36}
$$

$$
\frac{V}{V_0}(V_{\mathrm{mol}}, T, \boldsymbol{p}) = \exp(p_m \operatorname{Tr}(\ln_{\mathrm{M}}(\boldsymbol{F}_m(V_{\mathrm{mol}}, T)))) = \prod_m \left(\frac{V}{V_{0m}}\right)^{p_m} = V\left(\prod_m V_{0m}^{p_m}\right)^{-1}
\tag{37}
$$

which demonstrates that the decomposition is consistent with the volume of the scalar equation of state. The endmember deformation gradient tensors are already defined (Section 3.2.1) as

$$
\ln_{\mathrm{M}} \boldsymbol{F}_m(V_{\mathrm{mol}}, T) = \Psi_{ijklm}(V_{\mathrm{mol}}, T)\delta_{kl}
\tag{38}
$$

where the fourth rank tensor Ψ for each endmember m can be contracted into Voigt form and has the symmetry of the crystal structure (Figure 2). If we let $(\ln_{\mathrm{M}} \boldsymbol{F})_{\mathrm{xs}}$ take a similar form
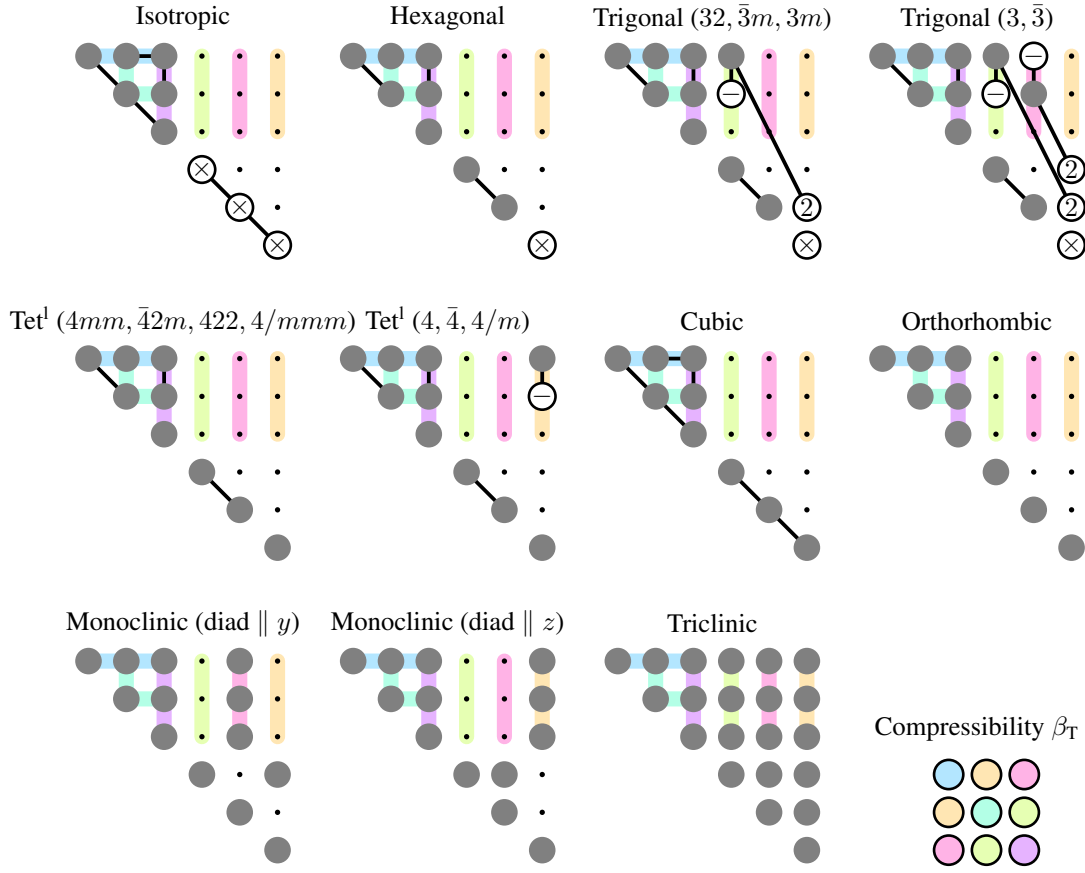
Figure 2. The forms of the (isothermal) elastic tensors for different types of lattice Nye et al. (1985). Thin black lines indicate a relationship between the connected components. Thick pastel-shaded lines indicate the three components that are summed to form the second order isothermal compressibility tensor (bottom right).

$$(\ln_{\mathrm{M}} \boldsymbol{F})_{\mathrm{xs}}(V_{\mathrm{mol}}, T, \boldsymbol{p}) = p_m p_n \mathbb{W}^{\Psi}_{ijklmn}(V_{\mathrm{mol}}, T, \boldsymbol{p}) \delta_{kl} \tag{39}$$

then we can express the deformation gradient at any composition as

$$\ln_{\mathrm{M}} \boldsymbol{F}(V_{\mathrm{mol}}, T, \boldsymbol{p}) = \Psi_{ijkl}(V_{\mathrm{mol}}, T, \boldsymbol{p}) \delta_{kl} \tag{40}$$

$$\Psi_{ijkl}(V_{\mathrm{mol}}, T, \boldsymbol{p}) = p_m \Psi_{ijklm}(V_{\mathrm{mol}}, T) + p_m p_n \mathbb{W}^{\Psi}_{ijklmn}(V_{\mathrm{mol}}, T, \boldsymbol{p}) \tag{41}$$

The cell tensor at any molar volume and temperature can be found by combining Equations 32, 33 and 40. The thermal expansivity α and isothermal compressibility β_{T} at fixed composition can be found using Equations 12, 14 and 40, and the isothermal compliance tensor $\mathbb{S}_{\mathrm{T}}$ can be calculated using Equations 27–30 and 41.

4 APPLICATION TO THE PLAGIOCLASE FELDSPARS

4.1 Introduction

Plagioclase feldspars are a dominant mineral group in the crust. Most plagioclase feldspars are well-approximated by a mix of two different chemical components, an albitic component with composition $NaAlSi_3O_8$ and an anorthitic component with composition $CaAl_2Si_2O_8$. They are triclinic, which makes them an ideal example solid solution to demonstrate the anisotropic equation of state introduced in this paper.

Plagioclase feldspars change space group depending on their composition, pressure and temperature of equilibration. Endmember anorthite adopts the $P\bar{1}$ space group, anorthite-rich ($p_{an} > 0.5$) plagioclases adopt the ordered $I\bar{1}$ space group, and albite-rich plagioclases adopt the disordered $C\bar{1}$ space group. The $I\bar{1}$ field shrinks relative to the $C\bar{1}$ field with increasing temperature but expands with increasing pressure, a consequence of the lower configurational entropy and molar volume of the $I\bar{1}$ phase.

Structural and elastic data for plagioclase crystals across the albite-anorthite binary have been collected by Angel et al. (1990) and Brown et al. (2006, 2016), and these data are used here to create an anisotropic model for the disordered $C\bar{1}$ (high) plagioclases. Extension to the $I\bar{1}$ space group is left for a future study, given the need to develop an anisotropic Landau-theory consistent with the equation of state (Carpenter, 1988; Dubacq, 2022).

4.2 Endmember and solution volumes

Endmember properties for albite and anorthite were taken from the dataset of (Stixrude & Lithgow-Bertelloni, 2022). These were then adjusted to best fit the data for $C\bar{1}$ plagioclases. As elastic properties across the solid solution have only been collected at room temperature and near-room pressure, only the V_0 and K_{T0} parameters were modified.

The excess properties across the solid solution were modelled as a symmetric (regular) binary solution. A constant volume excess term cannot accurately reproduce both the variation of V and K_{TR} across the solution, and so the volume excess was modelled by creating two new intermediate endmembers, one (aban1) with V_0, K_0 and K_0' equal to the average of the albite values, and a second (aban2) where V_0 and K_0 were allowed to vary. The volume was then modelled as:

$$V(p_{an}) = (1 - p_{an})V(ab) + (p_{an})V(ab) + 4(1 - p_{an})(p_{an})(V(aban2) - V(aban1)) \quad (42)$$

The fitted endmember and mixing properties are provided in Table 2. Because aban1 is derived from the properties of the ab and an endmembers, there are only three free variables for each endmember

	ab	an	aban (1)	aban (2)
V_0 (cm^3/mol)	9.996982e+01	1.011748e+02	1.005723e+02	1.007619e+02
K_0 (GPa)	5.521841e+01	8.845259e+01	7.183550e+01	7.902757e+01

Table 2. Standard state endmember and mixing properties

(six in total). The resulting standard state volumes and Reuss isothermal bulk moduli are plotted in Figure 3.
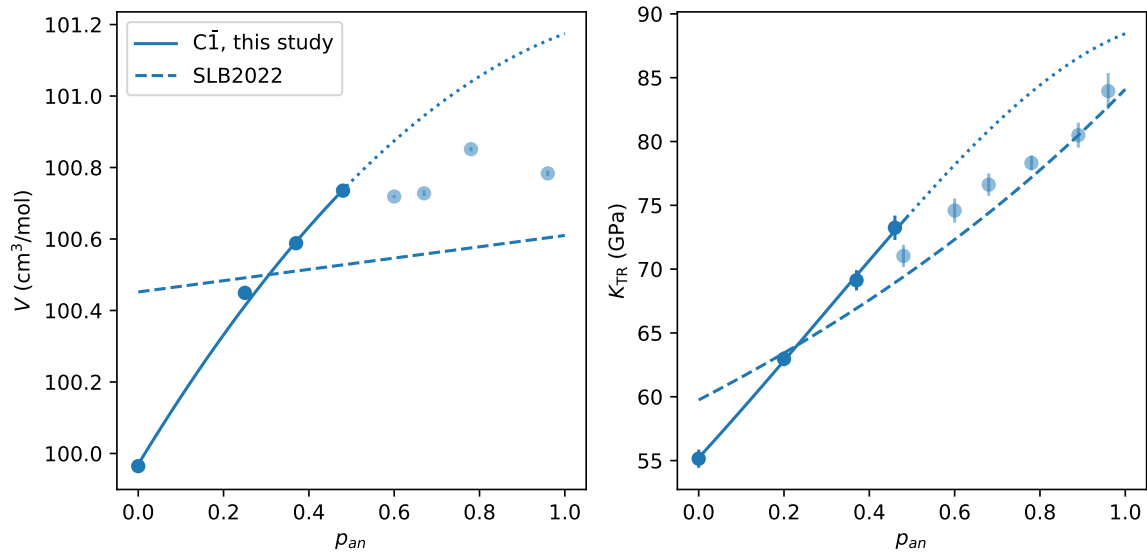
Figure 3. Plagioclase molar volumes and isothermal Reuss bulk moduli under standard state conditions. Data taken from Brown et al. (2016). The molar volumes in the $\bar{I1}$ and $\bar{P1}$ phases have been divided by two to allow direct comparison. The solid line represents the predictions for $C\bar{1}$ plagioclase from the model presented in this study. The dotted extension marks the region of compositional space where the $C\bar{1}$ structure is unstable. Dashed lines show the predictions of the thermodynamic model presented in Stixrude & Lithgow-Bertelloni (2022), which is a good fit to the data considering the goal of providing a single, simple solution model across the whole binary, but does not capture trends required to accurately reproduce the full elastic tensor across the binary.

	a (m)	b (m)	c (m)	α (°)	β (°)	γ (°)
ab	4.328825e-02	6.802831e-02	3.806904e-02	9.424428e+01	1.165933e+02	8.779559e+01
an	4.368841e-02	6.893277e-02	3.752945e-02	9.266318e+01	1.160068e+02	9.274265e+01

Table 3. Standard state endmember molar cell parameters.

4.3 Cell parameters

Anisotropic model parameters in this study are all treated as ideal; in other words, every element in the tensor $\mathbb{W}^{\psi}_{ijklmn}$ in Equation 41 is equal to zero. All the anisotropic properties across the binary are calculated using endmember M_0 and ψ functions.

The standard state molar cell tensor M_0 for each endmember is calculated from the molar cell parameters in Table 3 (see also Section 2). Because $V_0 = \det(M_0)$, there are only five free variables for each endmember (10 variables in total). The resulting cell properties across the binary are shown in Figure 4.
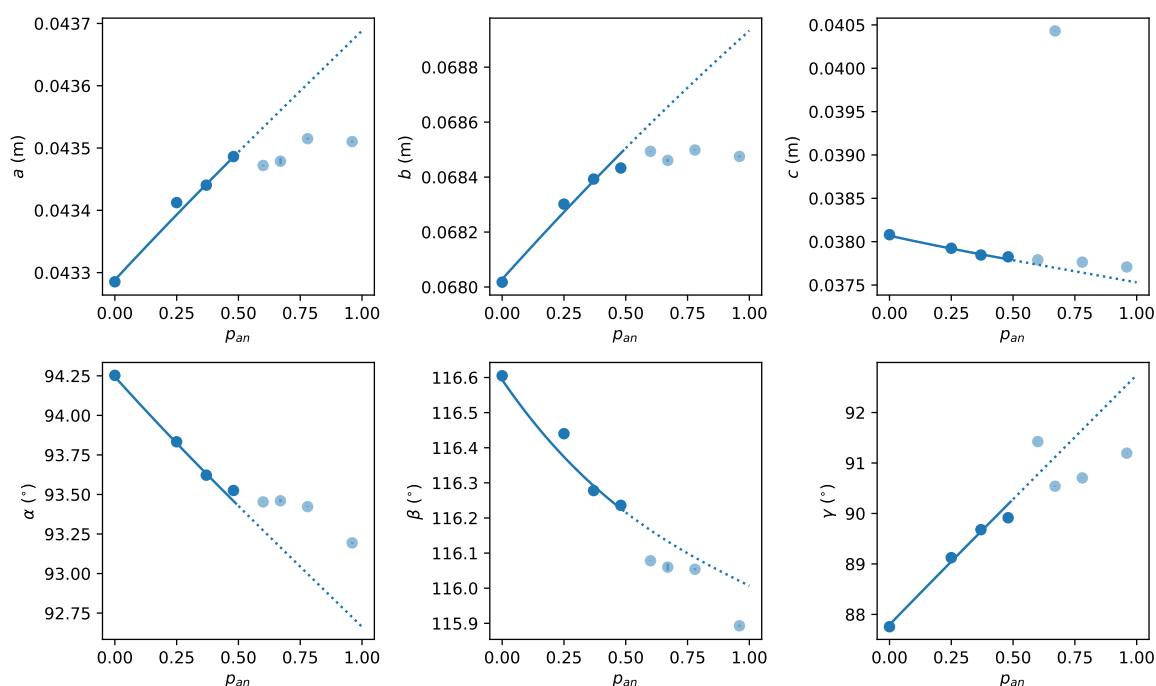
Figure 4. Plagioclase cell parameters under standard state conditions. Data taken from Brown et al. (2016). The c-axis lengths in the I$\bar{1}$ and P$\bar{1}$ phases have been divided by two to allow direct comparison. Solid and dotted lines represent the predictions for C$\bar{1}$ plagioclase from the model presented in this study, in the regions where C$\bar{1}$ is stable (solid lines) and metastable (dotted lines).

$$
A(\text{ab}) = \begin{pmatrix}
1.01031 & -0.19103 & -0.20793 & -0.34891 & 0.05814 & -0.14800 \\
-0.19103 & 0.36267 & 0.03256 & 0.16538 & 0.09163 & 0.09251 \\
-0.20793 & 0.03256 & 0.35983 & 0.21482 & -0.08675 & 0.14627 \\
-0.34891 & 0.16538 & 0.21482 & 2.59013 & 0.17605 & 0.62809 \\
0.05814 & 0.09163 & -0.08675 & 0.17605 & 2.12909 & -0.00734 \\
-0.14800 & 0.09251 & 0.14627 & 0.62809 & -0.00734 & 1.82348
\end{pmatrix}
\tag{44}
$$

Table 4. Voigt-form matrix describing the anisotropic properties of albite in the model presented in the text.

4.4 Elastic properties

As the data used in the inversion in this study is all collected at room pressure and temperature, the simplest formulation for Ψ can be adopted, whereby:

$$
\Psi_{ijkl} = p_m A_{mijkl} \ln\left(\frac{V}{V_{0m}}\right)
\tag{43}
$$

The elements of the tensor A_{mijkl} for each endmember m have the symmetries of an elastic compliance tensor, and so can be written in Voigt form (21 parameters for each endmember for triclinic symmetry). The only other requirement of this tensor is that $A_{mijkl}\delta_{ij}\delta_{kl} = 1_m$ (Equation 20), leaving 20 free variables for the two endmembers (40 variables in total). Values are provided in Tables 4 and 5.

4.5 Data inversion

Inversion of the data to obtain model parameters was performed in several parts:

- An approximation to the scalar V(P,T) equation of state was obtained by fitting the parameters in Section 4.2 to the volume and Reuss isothermal bulk modulus data.
- Approximate endmember cell parameters were found (Section 4.3), fixing the scalar parameters found in the previous step.
- Approximate endmember elastic parameters were found (Section 4.4) by fitting to the elastic

$$
A(\text{an}) = \begin{pmatrix}
0.83668 & -0.31243 & -0.18527 & -0.30773 & -0.06670 & -0.09333 \\
-0.31243 & 0.54310 & -0.02412 & 0.19836 & -0.02573 & 0.16298 \\
-0.18527 & -0.02412 & 0.66384 & -0.12707 & -0.11676 & 0.12377 \\
-0.30773 & 0.19836 & -0.12707 & 4.27238 & -0.06510 & 0.19217 \\
-0.06670 & -0.02573 & -0.11676 & -0.06510 & 2.41180 & -0.24125 \\
-0.09333 & 0.16298 & 0.12377 & 0.19217 & -0.24125 & 2.56196
\end{pmatrix}
\tag{45}
$$

Table 5. Voigt-form matrix describing the anisotropic properties of anorthite in the model presented in the text.
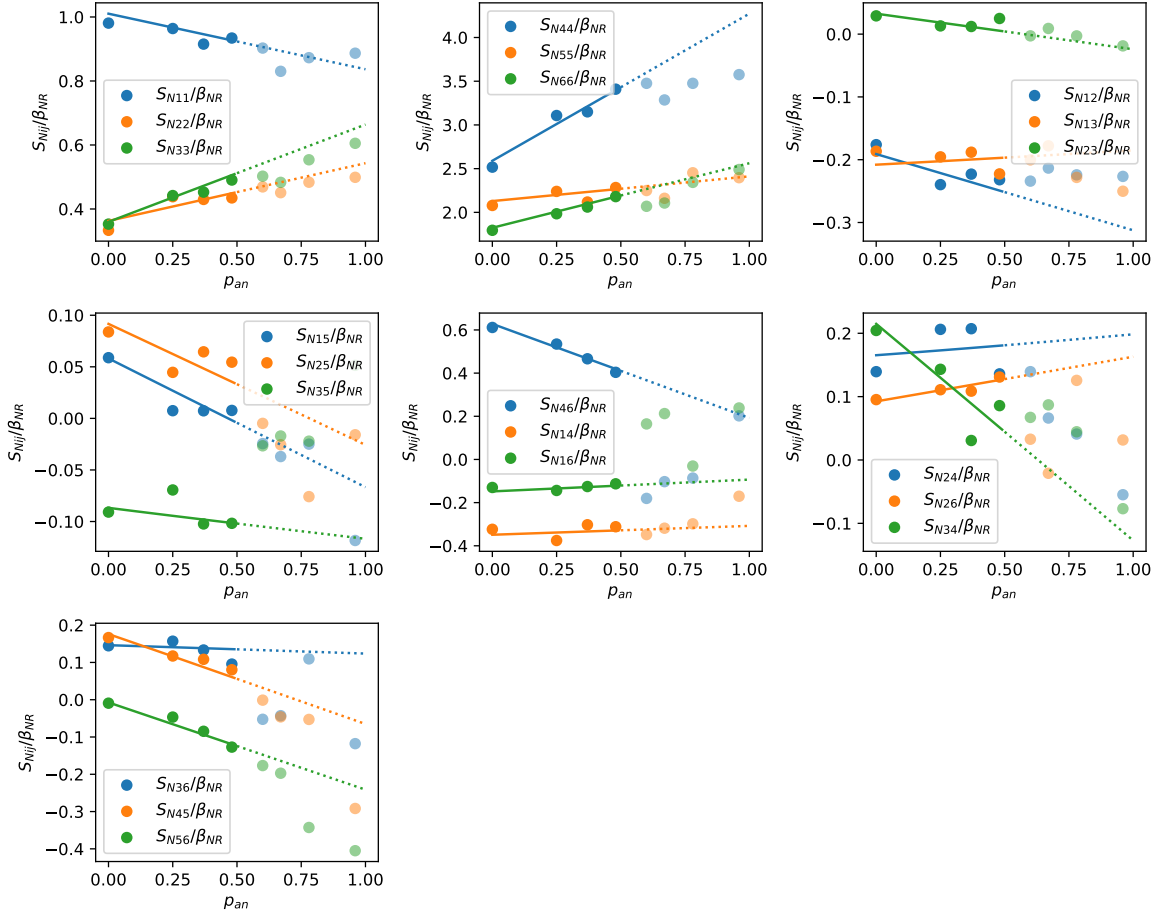
Figure 5. Plagioclase isentropic compliances divided by the isentropic Reuss compressibility under standard state conditions. Data taken from Brown et al. (2016). Solid and dotted lines represent the predictions for $C\bar{1}$ plagioclase from the model presented in this study, in the regions where $C\bar{1}$ is stable (solid lines) and metastable (dotted lines).

data. Because the relationship between the model parameters and the elements of the elastic stiffness tensor are highly nonlinear, it was found to be much more efficient to initially fit the ratio of isentropic compliances to isentropic Reuss compressibilities (Figure 5), which bear a near 1:1 relationship with the tensors A (Equations 27–30, Equation 43).

- Finally, all 56 parameters were simultaneously inverted using all the available data and uncertainties, including the isentropic elastic tensors (Figure 6).
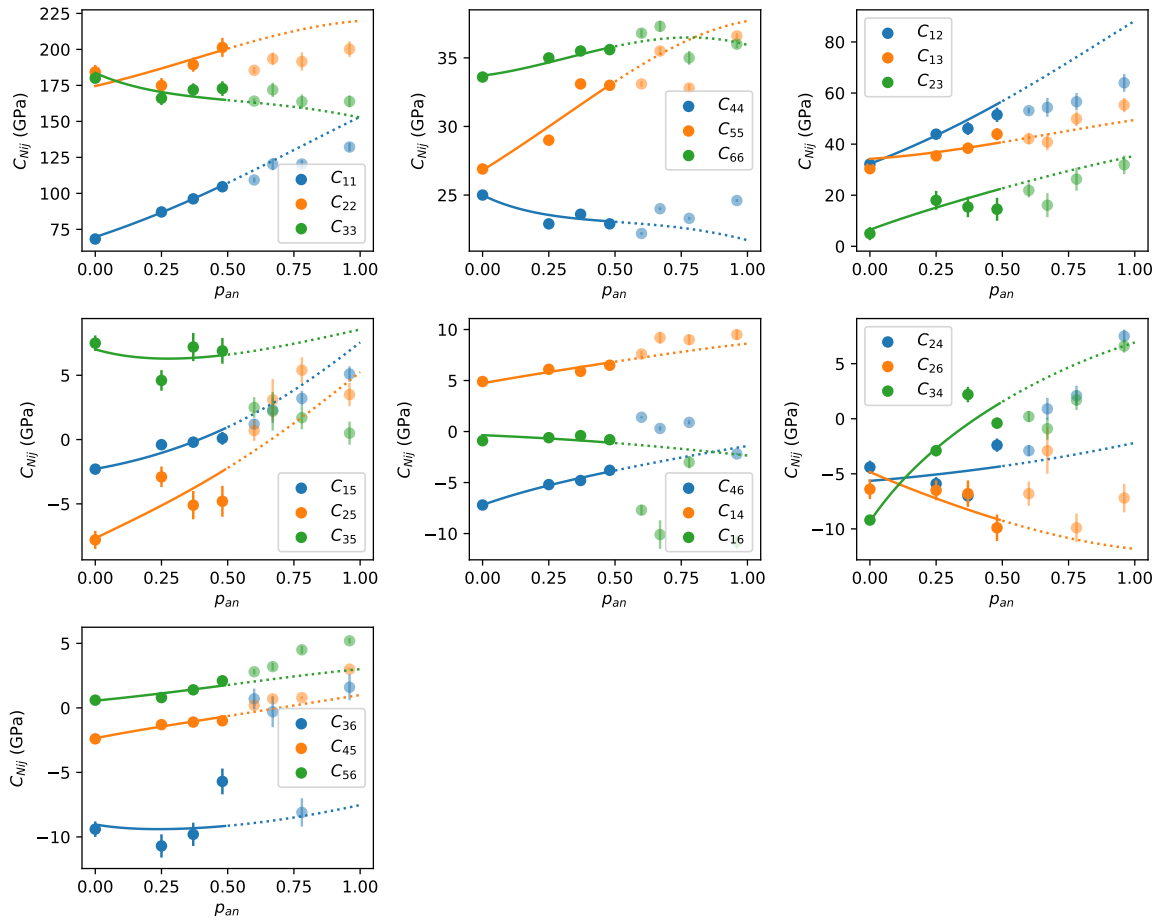
Figure 6. Plagioclase isentropic stiffnesses under standard state conditions. Data taken from Brown et al. (2016). Solid and dotted lines represent the predictions for C$\bar{1}$ plagioclase from the model presented in this study, in the regions where C$\bar{1}$ is stable (solid lines) and metastable (dotted lines).

4.6   Observed data versus model predictions

Overall, the fit between the observed data and model predictions is extremely good. This is perhaps not surprising, given the large number of fitting parameters (56) versus the number of data points (116). However, the good fit does suggest that treating the mixing of the anisotropic tensor as ideal (as done here) is suitable even when the solutions are volumetrically non-ideal. In addition, the model does draw out some nice contrasts between the $C\bar{1}$ and $I\bar{1}$ properties; in particular, the kink in volume and cell parameters at the phase boundary ($p_{\mathrm{an}} \sim 0.5$) and abrupt drop in isothermal bulk modulus (Figures 3 and 4). Also of interest are the near linear trends in $S_{\mathrm{N}ij}/\beta_{\mathrm{NR}}$ (Figure 5). Linearity in these trends (at constant V and T) is a prediction of the ideal anisotropic model, and so it is comforting to see that the simple model formalism does a good job at representing the data.

The second order isothermal compressibility tensors reported by (Angel, 2004) and Brown et al. (2016) were not used in the creation of the anisotropic model. This is because the isothermal compressibility tensor is very closely related to the isothermal elastic tensor (Equation 25), which in turn is closely related to the isothermal elastic tensor (at 0 K the two are identical). A comparison between the isothermal compressibilities reported by Brown (2018) and the model predictions are presented in Figure 7. Note that while the values of the compressibilities are reasonable, the trends of $\beta_{\mathrm{T}2}$, $\beta_{\mathrm{T}3}$ and $\beta_{\mathrm{T}6}$ are in poor agreement with the data, suggesting minor conflict between the high pressure unit cell data and the elastic tensor.

5   CONCLUSIONS

There has been a concerted effort in the last decade or so to provide elastic moduli for a range of materials at elevated pressure. Data at high pressure and temperature is still sparse, but as it grows, so too will the need for models that can reproduce this data in a format conducive to further work. The equation of state proposed in this paper has the benefit of being compact, self-consistent, and can be appended to preexisting V(P,T) equations of state.

Not included in this paper is any treatment of isochemical variation. Isochemical variation can include order-disorder of chemical species on sites (e.g., Al and Si in plagioclase; Carpenter, 1988), or structural flexibility (e.g., tetrahedral tilting in plagioclase; Mookherjee et al., 2016; Lacivita et al., 2020), or variation in proportions of spin states (e.g., iron in ferropericlase; Wu et al., 2013). Changes in isochemical state driven by changes in pressure or temperature can occur rapidly on the timescales of observations or natural phenomena such as seismic waves, and result in anomalous thermodynamic behaviour such as elastic softening. Plagioclase is one phase exhibiting such anomalous properties
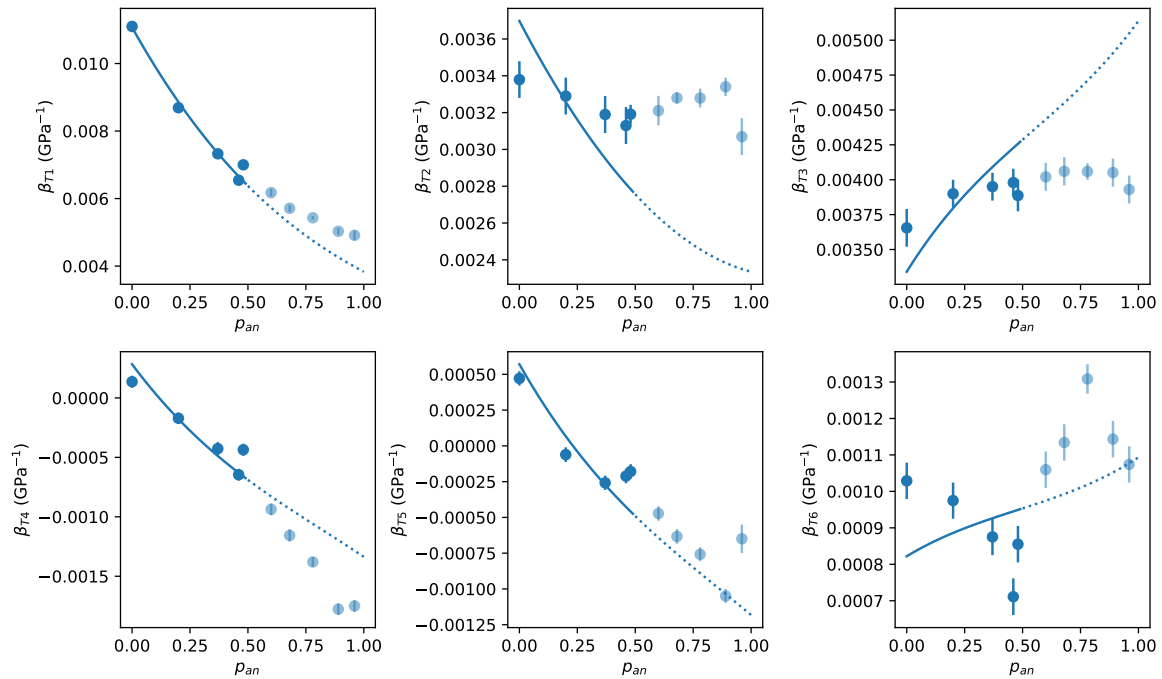
Figure 7. Plagioclase isothermal compressibilities under standard state conditions. Data taken from Brown et al. (2016). The observed values of the 4th, 5th and 6th compressibilities are all divided by two relative to the reported values, as Brown et al. (2016) reports the sum of elements of the Voigt-form compliance matrix, and elements of the off-diagonal 3x3 block of the Voigt-form compliance matrix are multiplied by two relative to the full compliance tensor. Solid and dotted lines represent the predictions for $C\bar{1}$ plagioclase from the model presented in this study, in the regions where $C\bar{1}$ is stable (solid lines) and metastable (dotted lines).

(Carpenter, 1988; Mookherjee et al., 2016; Lacivita et al., 2020). A treatment of isochemical variations in anisotropic solid solutions will be the subject of a follow up study.

ACKNOWLEDGMENTS

DATA AVAILABILITY

The anisotropic equation of state described in this paper is provided as a contribution to the BurnMan open source software project: `https://github.com/geodynamics/burnman` (Cottaar et al., 2014; Myhill et al., 2023).

References

Angel, R. J., 2004. Equations of state of plagioclase feldspars, *Contributions to Mineralogy and Petrology*, **146**(4), 506–512.

Angel, R. J., Carpenter, M., & Finger, L., 1990. Structural variation associated with compositional variation and order-disorder behavior in anorthite-rich feldspars, *American Mineralogist*, **75**(1-2), 150–162.

Brown, J., Abramson, E., & Angel, R., 2006. Triclinic elastic constants for low albite, *Physics and Chemistry of Minerals*, **33**(4), 256–265.

Brown, J. M., 2018. Determination of elastic moduli from measured acoustic velocities, *Ultrasonics*, **90**, 23–31.

Brown, J. M., Angel, R. J., & Ross, N. L., 2016. Elasticity of plagioclase feldspars, *Journal of Geophysical Research: Solid Earth*, **121**(2), 663–675.

Carpenter, M., 1988. Thermochemistry of aluminium/silicon ordering in feldspar minerals, in *Physical properties and thermodynamic behaviour of minerals*, pp. 265–323, Springer.

Cottaar, S., Heister, T., Rose, I., & Unterborn, C., 2014. Burnman: A lower mantle mineral physics toolkit, *Geochemistry, Geophysics, Geosystems*, **15**(4), 1164–1179.

Dubacq, B., 2022. Thermodynamics of ordering and mixing in plagioclase feldspars: atomistic modelling in favour of landau theory, *Contributions to Mineralogy and Petrology*, **177**(10).

Haber, H. E., 2018. Notes on the matrix exponential and logarithm, *Santa Cruz Institute for Particle Physics, University of California: Santa Cruz, CA, USA*.

Helffrich, G. & Wood, B. J., 1989. Subregular model for multicomponent solutions, *American Mineralogist*, **74**(9-10), 1016–1022.

Holland, T. & Powell, R., 2003. Activity-composition relations for phases in petrological calculations: an asymmetric multicomponent formulation, *Contributions to Mineralogy and Petrology*, **145**, 492–501.

Lacivita, V., D'arco, P., Mustapha, S., Bernardes, D. F., Dovesi, R., Erba, A., & Rérat, M., 2020. Ab initio compressibility of metastable low albite: revealing a lambda-type singularity at pressures of the Earth's upper mantle, *Physics and Chemistry of Minerals*, **47**(10), 1–13.

Mookherjee, M., Mainprice, D., Maheshwari, K., Heinonen, O., Patel, D., & Hariharan, A., 2016. Pressure induced elastic softening in framework aluminosilicate- albite (NaAlSi3O8), *Scientific Reports*, **6**(1), 34815.

Myhill, R., 2018. The elastic solid solution model for minerals at high pressures and temperatures, *Contributions to Mineralogy and Petrology*, **173**(2), 1–17.

Myhill, R., 2022. An anisotropic equation of state for high pressure, high temperature applications, *Geophysical Journal International*.

Myhill, R. & Connolly, J. A., 2021. Notes on the creation and manipulation of solid solution models, *Contributions to Mineralogy and Petrology*, **176**(10), 1–19.

Myhill, R., Cottaar, S., Heister, T., Rose, I., Unterborn, C., Dannberg, J., & Gassmoeller, R., 2023. BurnMan – a Python toolkit for planetary geophysics, geochemistry and thermodynamics, *The Journal of Open Source Software*, **8**(87), 5389.

Nye, J. F. et al., 1985. *Physical properties of crystals: their representation by tensors and matrices*, Oxford University Press.

Petersen, K. B. & Pedersen, M. S., 2012. The matrix cookbook, Version 20121115.

Stixrude, L. & Lithgow-Bertelloni, C., 2005. Thermodynamics of mantle minerals - I. Physical properties, *Geophysical Journal International*, **162**, 610–632.

Stixrude, L. & Lithgow-Bertelloni, C., 2011. Thermodynamics of mantle minerals - II. Phase equilibria, *Geophysical Journal International*, **184**, 1180–1213.

Stixrude, L. & Lithgow-Bertelloni, C., 2022. Thermal expansivity, heat capacity and bulk modulus of the mantle, *Geophysical Journal International*, **228**(2), 1119–1149.

Wu, Z., Justo, J. F., & Wentzcovitch, R. M., 2013. Elastic anomalies in a spin-crossover system: Ferropericlase at lower mantle conditions, *Physical Review Letters*, **110**(22).

This paper has been produced using the Blackwell Scientific Publications GJI LATEX2e class file.